

Symmetry broken states at high displacement fields in ABA trilayer graphene

Simrandeep Kaur¹, Unmesh Ghorai², Abhisek Samanta³, Kenji Watanabe⁴,
Takashi Taniguchi⁵, Rajdeep Sensarma⁶, Aveek Bid^{1*}

¹*Department of Physics, Indian Institute of Science, Bangalore 560012, India*

²*School of Physics and Astronomy, Tel Aviv University, Tel Aviv 6997801, Israel*

³*Department of Physics, Indian Institute of Technology Gandhinagar, Gujarat 382355,
India*

⁴*Research Center for Functional Materials, National Institute for Materials Science, 1-1
Namiki, Tsukuba 305-0044, Japan*

⁵*International Center for Materials Nanoarchitectonics, National Institute for Materials
Science, 1-1 Namiki, Tsukuba 305-0044, Japan*

⁶*Department of Theoretical Physics, Tata Institute of Fundamental Research, Homi
Bhabha Road, Mumbai, 400005, India*

E-mail: aveek@iisc.ac.in

Abstract

We present a comprehensive study of magnetotransport in high-mobility trilayer graphene (TLG) devices under a transverse displacement field, focusing on symmetry-broken Landau levels (LLs) from monolayer-like and bilayer-like bands. A striking displacement-field-induced enhancement of the Landé g-factor is observed in the zeroth Landau level of the monolayer-like band, highlighting the formation of interaction-driven quantum Hall states. Additionally, we find a rich landscape of LL crossings

in the Dirac gully region, accompanied by phase transitions between spin-, gully-, and valley-polarized LLs. These experimental observations are successfully modeled using calculations based on optimized tight-binding parameters. Furthermore, our results reveal significant particle-hole asymmetry in the sequence of LLs in the Dirac gullies, attributed to differing g-factor values for electrons and holes. This asymmetry underscores the limitations of non-interacting models in capturing the complexities of multiband systems. This work provides new insights into the interplay of symmetry-breaking mechanisms and enhanced interaction effects in Bernal-stacked trilayer graphene, advancing our understanding of quantum transport phenomena in multiband systems.

Introduction

Bernal-stacked trilayer graphene (TLG) is a distinctive condensed matter platform to investigate lattice symmetries and tune them using external parameters like magnetic and displacement fields¹⁻⁵. In its pristine form, TLG is a semi-metallic multiband system formed by a massless monolayer-like (ML-like) band and massive bilayer-like (BL-like) bands (Fig. 1(a)), protected from inter-mixing by the lattice mirror symmetry⁶⁻⁸. An external perpendicular displacement field D introduces a potential difference Δ_1 between its top and bottom carbon layers, breaking the mirror symmetry and hybridizing the ML-like and the BL-like bands^{2,6}. This dual-band structure, unique among layered material provides a platform to explore multiband phenomena, especially in the regime where spin, valley and layer degree of freedoms are entangled.

In the single-particle picture, Δ_1 , along with the interlayer skewed hopping term γ_3 , cause strong trigonal warping of the low-energy spectrum, producing a set of additional off-center low-energy Dirac cones termed as Dirac gullies with C_3 rotational symmetry^{6,8-10}. They are labeled as T_1 and T_2 over the electron side, and T_3 and T_4 over the hole side (Fig. 1(b)). An external electric field can tune the strength of these Dirac gullies and also modulate their effective mass, significantly changing their structure at low energies^{6,8,11}. These gullies

also provide a rich ground for the emergence of correlated phases, including gully polarized nematic phase^{6,10}, inter gully tunneling with B_{perp} , chiral edge modes^{11,12}, multiple Lifshitz transitions^{8,9}.

In weak magnetic fields, such gullies lead to three-fold degenerate Landau levels with negligible tunneling between the gullies^{9,10}. At sufficiently large B_{\perp} , inter gully tunneling becomes so strong that the three-fold degeneracy of the LLs is completely lifted, driving the system into a magnetic breakdown regime. This lifting results in a rich sequence of phase transitions among symmetry-broken states involving spin, valley, and gully-polarized Landau levels. Despite strong theoretical predictions^{6,8,11} the experimental realization of these gullies, mapping of these phases, and the role of electron-electron interactions in the high magnetic field regime remains largely unexplored. This is partly due to the need for devices with exceptionally low disorder, where the subtle differences between the closely lying ground states may be discerned.

In this work, we bridge the existing gap by performing detailed magnetotransport studies on high-mobility TLG devices, enabling us to systematically explore the complex landscape of symmetry broken states arising from both the monolayer-like and bilayer-like bands. We observe a surprising displacement-field-induced enhancement of the Landé g-factor in the zeroth Landau level of the monolayer-like band. This enhancement is accompanied by a spontaneous SU(4) symmetry breaking in the bilayer-like LLs, strongly suggesting the formation of interaction-driven quantum Hall states. Furthermore, we investigate the rich pattern of LL crossings in the Dirac Gully region, revealing the multiple-phase transitions between spin, Gully, and valley-polarized LLs in the high field regime(B_{\perp}). These transitions are the hallmarks of the magnetic breakdown regime, where inter-gully tunneling lifts the triplet degeneracy. We map all the experimentally observed transport features with our calculations based on optimized non-interacting tight-binding parameters^{8,9}. Interestingly, our experimental results reveal a pronounced asymmetry in the evolution of LLs in the Dirac gullies at positive and negative energies; we establish that this particle-hole asymmetry

arises from the stark distinction in the values of the g-factor for electrons and holes. Our study highlights the underlying imbalance in interaction effects across different gullies and inadequacy of a single-particle picture in capturing the physics of symmetry-broken quantum Hall states in TLG.

Results

Bernal-stacked trilayer graphene flakes referred to as TLG, mechanically exfoliated on SiO_2 , were identified through optical contrast and Raman spectroscopy¹³. TLG devices encapsulated with hBN with graphite gates (Fig. 1(c)) were prepared using the dry transfer technique^{14–16}. Dual electrostatic gates were used to tune the number density n and the displacement field D simultaneously, see Supplementary Information, section **S1**¹⁷. Line plots of longitudinal resistance versus back gate voltage at different top gate voltages, shown in Fig. 1(d), confirm the device channel to be of ABA stacked TLG, evidenced by the minimal change in the resistance with displacement fields¹⁸.

A contour map of the derivative of the longitudinal conductance $dG_{xx}/dn(B = 0)$ at $T = 20$ mK in the charge carrier density $n - D$ plane is shown in Fig. 1(e). We encounter various discontinuities in the dG_{xx}/dn that evolve with the displacement field and the number density. The charge neutrality point is the dashed line marked **A**. With increasing D , the monolayer-like bands are predicted to shift to higher energies^{2,19}. The two linearly dispersing lines on both the electron and hole sides marked as **E** trace this evolution of the extrema of the monolayer-like bands with D . The features marked by lines **B**, **C**, and **D** arise from the multiple Lifshitz transitions due to modification in the BL-like bands⁹. Although seen through Quantum capacitance measurements, these signatures of the Lifshitz transition in TLG had eluded previous transport studies. The detailed Fermi contours in different regions of the $n - D$ plot are shown in the Supplementary Information section **S2**¹⁷. Data obtained on another device with qualitatively similar observations are shown in

Supplementary Information section **S3**¹⁷.

In the Quantum Hall regime, the Lifshitz transitions lead to changes in the LL filling sequence and are discernible as sharp discontinuities in the Landau fan diagrams. Fig. 1(f) shows the evolution of the minima of R_{xx} in a perpendicular magnetic field $B = 2$ T in the ν - D plane. Here, $\nu = nh/eB$ is the LL filling factor, h is the Planck's constant and e is the magnitude of electronic charge. The sequence of ν changes abruptly by 2 across the dashed line **E** as a consequence of the LL order changing from 4ν to $4(\nu + 1/2)$ as the BL-like LLs cross the ML-like LLs^{19,20}. In the regions marked by **B'**, **C**, the formation of C_3 symmetric Dirac cones leads to the emergence of Landau level spaced by three (Fig. 1(f)).

Fig. 2(a) shows the Landau fan diagram at $D = 0$ and $T = 5$ K. The LLs of the bilayer sector emerge from $n = 0$. The four LLs emerging from $n = 0.5 \times 10^{16} \text{ m}^{-2}$ are the spin and valley non-degenerate quartet of the zeroth LL of the ML band, labeled $N_M = 0$ ^{3,4}. The intersection of the $N_M = 0$ and the BL-like LL $N_B = 2$ near $B = 4$ T gives rise to the pattern highlighted by the white dotted ellipse.

As noted before, D -field mixes the ML-like and BL-like bands, causing them to lose their pure ML-like and BL-like characters^{6,21}. However, referencing the LLs at high D , we retain the same notations at $D = 0$ V/nm for consistency. In Fig. 2(d), we plot the Landau fan diagram measured at $D = 0.75$ V/nm. We observe that the position of the zeroth LL of the ML-like band originating from the K' -valley, $N_M = 0^-$ marked by white solid line changes little to $n \sim 0.7 \times 10^{16} \text{ m}^{-2}$ as compared to its position at $D = 0$. Conversely, the $N_M = 0^+$ which is the zeroth LL of the ML-like band in the K valley and marked as the dotted white line, moves to a significantly larger number density, $n \sim 3 \times 10^{16} \text{ m}^{-2}$. To account for the observed behavior, we calculated the LL spectrum of ABA TLG using tight binding parameters based on Slonczewski-Weiss-McClure model parameters^{8,22,23} with varying interlayer potential Δ_1 . For TLG, $\Delta_1 = -[(d_\perp/2\epsilon_{TLG}) \times D]e$ ^{9,12} leads to $\Delta_1(\text{eV}) = 0.084 D$ (V/nm). Here, $d_\perp = 0.67$ nm is the separation between the top and bottom layers of TLG, and ϵ_{TLG} is the dielectric constant of the TLG. The results are shown in Fig. 2(b)

for $\Delta_1 = 0$ meV ($D = 0$ V/nm) and Fig. 2(e) for $\Delta_1 = 60$ meV ($D \approx 0.75$ V/nm). They show that with increasing D , the conduction band of the monolayer sector localized at the K -valley, drifts to higher energies, whereas the valence band of the monolayer sector which is localized at the K' -valley remains unchanged; reproducing the observed experimental features. Note that in our calculations, LLs are spin non-degenerate with Landé g -factor of 2.

To investigate the impact of LL crossings on the energetics of the system, we measured the Zeeman gap between the $N_M = 0^+ \uparrow$ and $N_M = 0^+ \downarrow$ LLs at different values of D . Fig. 2(c) and Fig. 2(f) are the plots of longitudinal resistance R_{xx} versus ν in the vicinity of $N_M = 0^+$ LL measured at $D = 0$ V/nm and $D = 0.75$ V/nm respectively for $B = 10$ T. The shaded rectangles mark the resistance minima for the Fermi energy lying between the $N_M = 0^+ \uparrow$ and $N_M = 0^+ \downarrow$ LLs. An activated fit to the R_{xx} minima gives an estimate of the gap Δ between the spin-up and spin-down LLs: $R_{xx} = R_0 \exp(-\Delta/2k_B T)$ with $\Delta = g^* \mu_B B$. We find $\Delta = 2.15$ meV and 3.71 meV for $D = 0$ V/nm and 0.75 V/nm respectively, yielding $g^* \approx 4$ for $D = 0$ V/nm and $g^* \approx 6.3$ for $D = 0.75$ V/nm. Since activation measurements consistently underestimate the real gap²⁴, these numbers represent a lower limit of $g^*(D)$. The observation of the D -dependence of spin splitting motivates defining an ‘effective’ Landé g -factor $g^* \mu_B B = g \mu_B B + \mathcal{E}_{ex}^0(D)$ such that the Zeeman energy $E_Z = \sigma g^* \mu_B B$ ($\sigma = \pm 1/2$ for the two opposite spins). Here, μ_B is Bohr magneton, $g = 2$ is free electron g -factor, and $\mathcal{E}_{ex}^0(D)$ is the D -field dependent electron-electron interaction energy. In this picture, the increase in g^* with D reflects a commensurate increase in the electron-electron interaction energy. With increasing D , the BL-like LLs and the $N_M = 0^+$ LL approach each other. A enhanced electron-electron interaction will favor increased spacing between these LLs to minimize the repulsion between them. This, in turn, leads to an ‘effective’ increase of the g -factor. For details, see Supplementary Information, Section S4¹⁷ for details.

Support for interaction-induced enhancement of LL spacing comes from examining the areas marked by red dotted rectangles in Fig. 2(a,d). In panel (a), the region is away from

the crossing point of the BL-like and ML-like bands, and one observes that the BL-like LL are four-fold degenerate. In panel (d), by contrast, over the same range of magnetic fields but for $D = 0.75$ V/nm, all the degeneracies of the BL-like bands are lifted, indicating an enhancement of the spacing between the BL-like LLs as they cross the ML-like LL (for details, see Supplementary section **S4**¹⁷). This D -field induced lifting of the SU(4) symmetry of both BL-like and ML-like band was not seen previously in TLG²⁵ and provides us with the platform to tune the effective Landé g factor in the same system through a displacement field.

Focusing on the BL-like band, Fig. 3(a) shows the contour plot of G_{xx} as a function of magnetic field and filling factor ν at $D = 0.95$ V/nm and $T = 20$ mK. We observe multiple Landau level crossings that evolve with B . At low B , $G_{xx} = 0$ only at $\nu = \pm 6$ and ± 12 which is marked by white dashed lines. This is consistent with the emergence of six-fold degenerate states where three-fold LLs degeneracy comes from gully and spin. Increasing B lifts the gully and spin degeneracies, leading to multiple phase transitions among these broken symmetry states and driving the system to magnetic breakdown regime. Theoretically predicted^{6,8}, these phases had escaped experimental determination.

To understand the different phase transitions, we have calculated density of states plotted in Fig. 3(b). The LL crossings observed in the experimental data are faithfully reproduced by our calculations. The matched regions are marked by blue circles in Fig. 3(a) and (b). From the simulated plots in Fig. 3(c), we identify the LLs between $\nu = 12$ and 6 emerging from T_1 gully, $\nu = 6$ and 0 emerging from T_2 gully, $\nu = 0$ and -6 emerging from T_3 gully and those between $\nu = -6$ and -12 from T_4 gully.

As seen from Fig. 3(a), for positive energies, the first symmetry-broken LLs to be resolved are $\nu = 2, 4, 6$ in the T_2 gully and $\nu = 8, 10, 12$ in the T_1 gully; these are marked by green dashed lines in Fig. 3(a). Conversely, for negative energies, the LLs initially appear at $\nu = -3$, and -6 in T_3 gully and $\nu = -9$, and -12 in T_4 gully which are marked by purple dashed lines in Fig 3(a). The order of symmetry breaking of different gullies

with the magnetic field is thus non-trivial and is strongly particle-hole asymmetric. While the experimentally observed LL crossings in the T_1 and T_2 gullies conform to theoretical expectation, regions marked by blue ellipses in Fig. 3(a) and (b), those in the T_3 gully deviate from theoretical expectations. These regions are shown explicitly by yellow ellipses in Fig. 3(a) and (b).

This electron-hole asymmetry in the order of symmetry breaking is unexpected. According to the Landau spectrum obtained from a single particle picture which we have calculated assuming $g = 2$ is presented in Fig. 3(c), the valley degeneracy is lifted first, resulting in QH states at $\nu = \pm 6, \pm 12$. This is followed by the gully degeneracy lifting, which resolves additional filling factors at $\nu = \pm 2, \pm 4, \pm 8, \pm 10$. This framework aligns well with our observations at positive energies where G_{xx} minima occur at $\nu = 2, 4, 8, 10$. However, the observation of G_{xx} minima at $\nu = -3$ and $\nu = -9$ at negative energies suggests that for the holes, the spin degeneracy is lifted before the gully degeneracy. This is clearly shown in Fig 3(d) where spin degeneracy lifting between LLs marked by dashed line for down spin (\downarrow) and solid line for up spin (\uparrow) leads to $\nu = -3, -6$ LLs.

To address the observed discrepancy, we estimated the Landé g factor for the spin split LLs in both T_2 and T_3 gully (Supplementary Information, Section S6¹⁷). We found the effective g^* value for the T_3 gully is significantly enhanced to 6.31 while for T_2 gully, it is 2.99 which is closer to the bare value of 2. This substantial increase in the value of g^* for T_3 is a probable origin of the deviation of our experimental observations from the predictions of the non-interacting picture. Such discrepancies in the g^* values marks the imbalance in interaction effects for different gullies.

Based on our experimental data and simulations, we present a phase diagram of the gully region in the $\nu - B$ space in the magnetic breakdown regime shown in Fig. 4(a). $T_{\alpha\beta}^\gamma$ represents the gully LL with $\alpha = 1, 2$ the gully index, $\beta = 1, 2, 3$ the component of the triplet and $\gamma = \pm$ the valley index (Fig. 4(b)). The solid lines (dashed lines) represent the spin-up (spin-down) LLs. Increasing B at a fixed value of $\Delta_1 = 80$ meV leads to the braiding of the

LLs, as shown in Fig. 3(c), causing multiple phase transitions among the LLs having different spin, valley, and gully indices. Each symbol in Fig 4(c) corresponds to the pattern shown in Fig 4(a) and tracks the evolution of each LL with magnetic fields. The cyan-colored regions in Fig. 4(a) are the regions where the LLs are simultaneously spin and valley polarized. These are the regions where spin-split LLs from T_1 and T_2 gullies coexist. Similarly, the yellow areas host the spin-gully polarized state; here, spin-split LLs within the single gully coexist. The overlap between the calculated spectrum in Fig. 4(a) and the experimentally measured one (Fig. 4(c)) is apparent from the one-to-one correspondence between the regions marked by different symbols in the two plots.

In multiband systems with multiple valleys and gullies, it becomes important to directly probe these spin-polarized states. To examine the spin character, we have performed tilted field experiments (Supplementary section 10¹⁷). $B_{||}$ enhances the Zeeman splitting, increasing the spin gap. This results in more clearly resolved LL crossings under high $B_{||}$, further confirming the spin character of LLs.

Conclusions

In conclusion, we have investigated the symmetry-broken quantum Hall states in both monolayer and bilayer sectors of Bernal-stacked trilayer graphene at high displacement fields. In the monolayer band, high displacement fields enhance the spin splitting gap for $N_M = 0^+$ LLs. We attribute this enhancement to electron-electron interactions between ML-like and BL-like Landau levels, which additionally lead to complete degeneracy lifting of bilayer LLs near the crossing points and form the interaction-driven quantum Hall states. We have also explored the symmetry-breaking sequence of LLs in the Dirac gullies at high displacement fields and found a non-trivial gully polarized state with a strong electron-hole asymmetry. The displacement field dependence of the Zeeman splitting in trilayer graphene emphasizes the imbalance of interaction effects in different gullies and inadequacy of the often-used

non-interacting model in studying quantum transport in multiband systems.

AUTHOR INFORMATION

S. K. and A. B. conceptualized the study, performed the measurements, and analyzed the data. U.G., A.S., and R.S. performed the theoretical analysis. K.W. and T.T. grew the hBN single crystals. S.K., A.B., U.G., A.S., and R.S. contributed to preparing the manuscript.

Competing interests

The authors declare no competing financial interest.

Acknowledgement

A.B. acknowledges funding from U.S. Army DEVCOM Indo-Pacific (Project number: FA5209 22P0166). K.W. and T.T. acknowledge support from JSPS KAKENHI (Grant Numbers 19H05790, 20H00354, and 21H05233)

Data Availability

The data that supports the findings of this article are available from the authors upon reasonable request.

Supporting Information Available

Supporting information contains detailed discussions of (a) device fabrication and characterization details and (b) data on other devices.

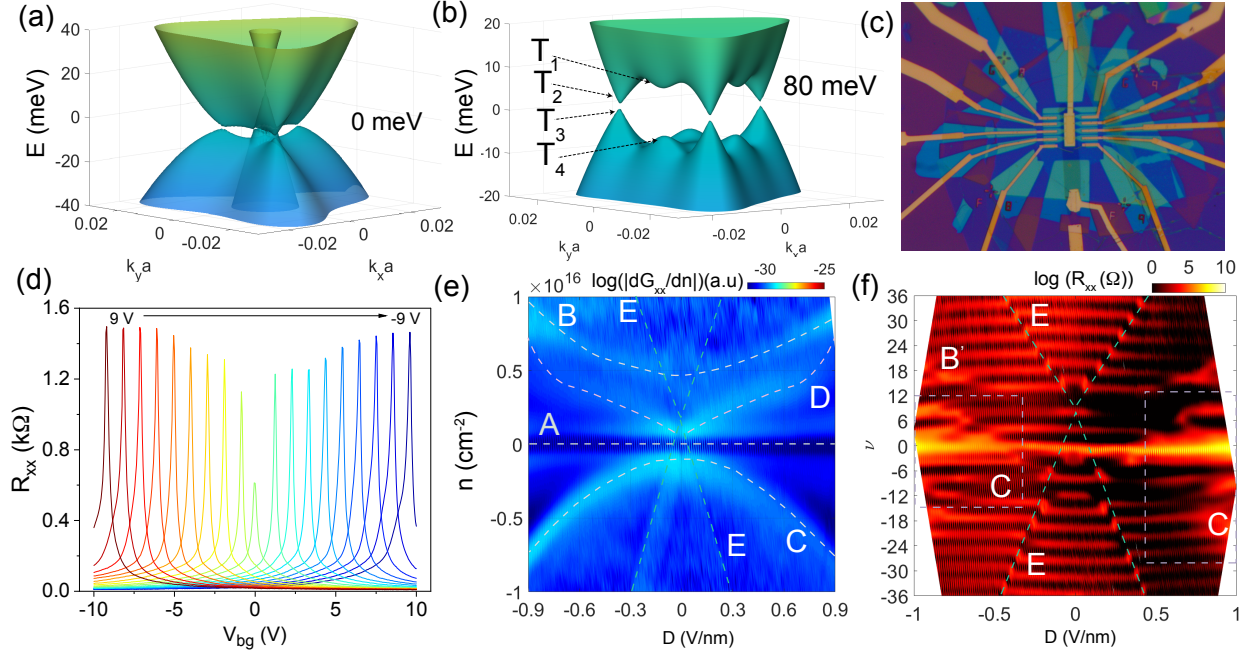


Figure 1: **Device characteristics:** (a) Calculated ABA trilayer graphene band structure at $D = 0$ meV. (b) Calculated band structure of ABA trilayer graphene at $D = 80$ meV. T_1 and T_3 Gullies are hosted by K valley, while T_2 and T_4 Gullies are in the K' valley⁸. (c) Optical image of the ABA trilayer graphene device. (d) Plots of R_{xx} versus V_{bg} for representative values V_{tg} at $T = 2$ K and $B = 0$ T. (e) Contour map of the derivative of the conductance, dG_{xx}/dn versus n and D . The dotted lines show the evolution of the charge neutrality point (A), the extrema of the monolayer-like bands (E), and several Lifshitz transitions (B, C and D). (f) Contour map of R_{xx} at $B = 2$ T.

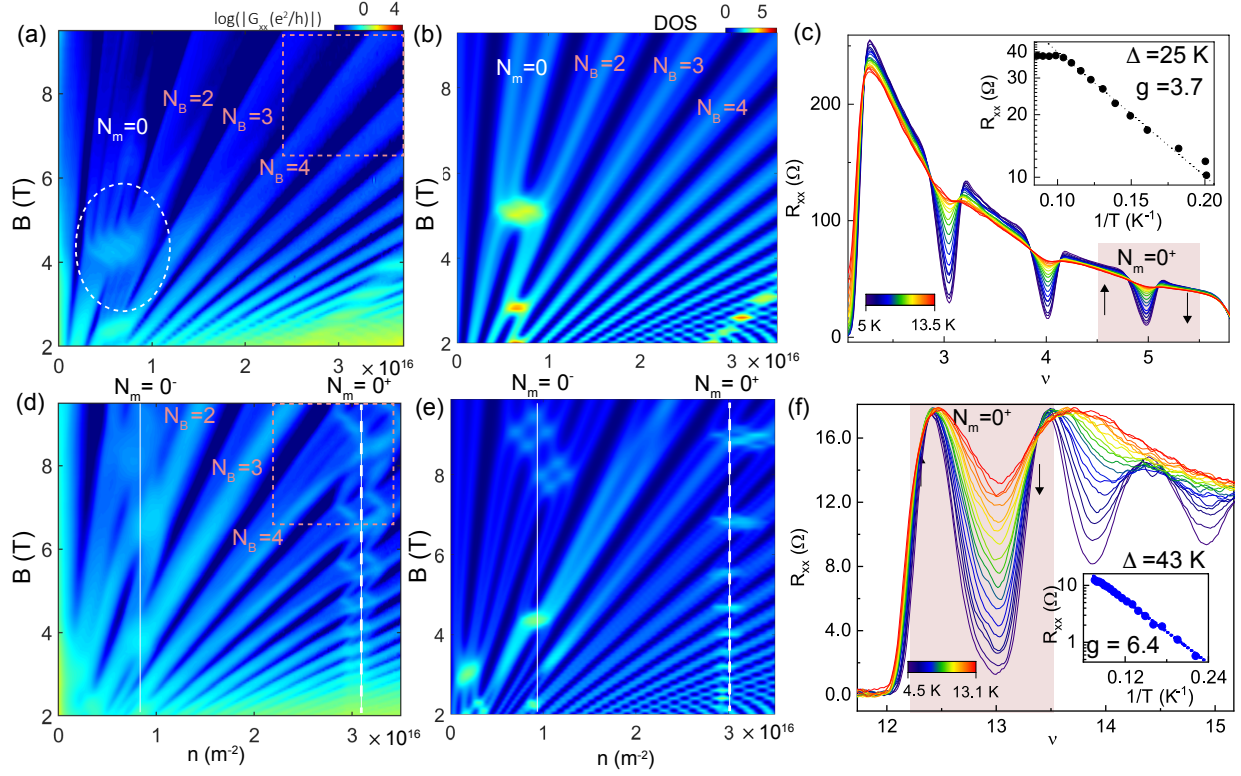


Figure 2: **Displacement field dependent fan diagrams:** Map of G_{xx} as a function of n and B at (a) $D = 0 \text{ V/nm}$, and (d) $D = 0.75 \text{ V/nm}$. The circle in (a) marks the crossing of $N_M = 0$ LL with $N_B = 2$ LL of the bilayer-like band. Simulated Landau level spectra for (b) $\Delta_1 = 0 \text{ meV}$ and (e) $\Delta_1 = 60 \text{ meV}$. The vertical solid lines in (d) and in (e) indicate the positions of the spin-degenerate $N_M = 0^-$ ML-like LL. The solid dotted lines indicate the positions of the spin-degenerate $N_M = 0^+$ ML-like LL. Plot of R_{xx} as a function of filling factor ν at different temperatures for (c) $D = 0 \text{ V/nm}$, (f) $D = 0.75 \text{ V/nm}$. The shaded region marks the R_{xx} minima for $N_M = 0^+$ LL. Insets show the Arrhenius fits to the minima of R_{xx} as a function of $1/T$.

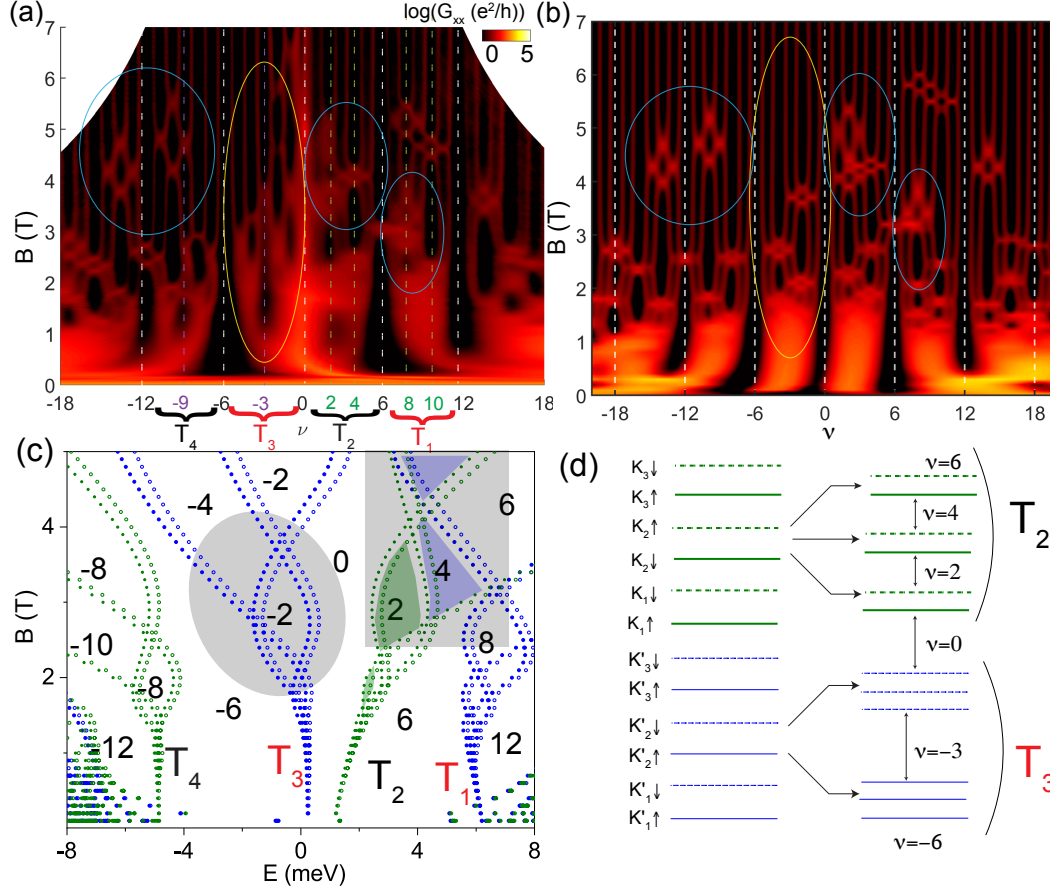


Figure 3: **Evolution of Landau levels near Dirac gullies:** (a) Measured contour map of G_{xx} as a function of ν and B measured at $D = 0.95$ V/nm. (b) Calculated contour map of the DOS as a function of ν and B at $\Delta = 80$ meV. Here D and Δ are related by $\Delta = \gamma D$ with $\gamma = 0.084$ e nm. The dark black regions correspond to vanishing DOS and hence conductance minima. The blue circles mark the regions of LL crossings in the experimental data and simulations. The yellow ellipse marks the region where simulated and experimental data diverge. (c) Simulated LL plot at $\Delta_1 = 80$ meV. T_1, T_2, T_3, T_4 are the gullies. The numbers in the plot are the filling factor ν . (d) Schematic showing the inferred order of spin and gully degeneracy breaking in the two gullies T_1 (on the electron) and T_2 (on the hole side).

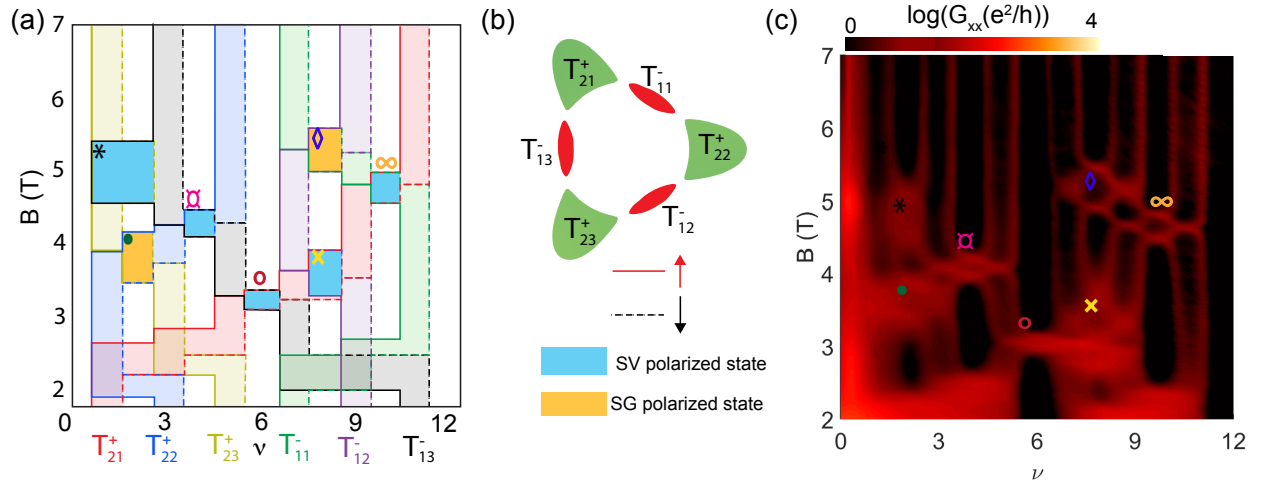


Figure 4: **Identification of filling sequence of QH states at high displacement fields:** (a) Evolution of LLs emerging from different gullies as a function of magnetic field and filling factor. The solid (dashed) line represents up spin LL (down spin LL). The cyan region hosts the spin and valley polarized states, and the yellow region hosts the spin and gully polarized states. Here, $T_{\alpha\beta}^\gamma$ represent the LL of the gully with γ as the valley index, α as the gully type, β is the index of LL within the single gully. (b) Calculated Fermi contour at $\Delta_1 = 80$ meV. (c) Contour plot of G_{xx} as a function of the magnetic field B and filling factor ν .

References

- (1) Campos, L. C.; Taychatanapat, T.; Serbyn, M.; Surakitbovorn, K.; Watanabe, K.; Taniguchi, T.; Abanin, D. A.; Jarillo-Herrero, P. Landau Level Splittings, Phase Transitions, and Nonuniform Charge Distribution in Trilayer Graphene. *Phys. Rev. Lett.* **2016**, *117*, 066601.
- (2) Datta, B.; Agarwal, H.; Samanta, A.; Ratnakar, A.; Watanabe, K.; Taniguchi, T.; Sensarma, R.; Deshmukh, M. M. Landau Level Diagram and the Continuous Rotational Symmetry Breaking in Trilayer Graphene. *Phys. Rev. Lett.* **2018**, *121*, 056801.
- (3) Datta, B.; Dey, S.; Samanta, A.; Agarwal, H.; Borah, A.; Watanabe, K.; Taniguchi, T.; Sensarma, R.; Deshmukh, M. M. Strong electronic interaction and multiple quantum Hall ferromagnetic phases in trilayer graphene. *Nature Communications* **2017**, *8*, 14518.
- (4) Stepanov, P.; Barlas, Y.; Espiritu, T.; Che, S.; Watanabe, K.; Taniguchi, T.; Smirnov, D.; Lau, C. N. Tunable Symmetries of Integer and Fractional Quantum Hall Phases in Heterostructures with Multiple Dirac Bands. *Phys. Rev. Lett.* **2016**, *117*, 076807.
- (5) Stepanov, P.; Barlas, Y.; Che, S.; Myhro, K.; Voigt, G.; Pi, Z.; Watanabe, K.; Taniguchi, T.; Smirnov, D.; Zhang, F.; Lake, R. K.; MacDonald, A. H.; Lau, C. N. Quantum parity Hall effect in Bernal-stacked trilayer graphene. *Proceedings of the National Academy of Sciences* **2019**, *116*, 10286–10290.
- (6) Serbyn, M.; Abanin, D. A. New Dirac points and multiple Landau level crossings in biased trilayer graphene. *Phys. Rev. B* **2013**, *87*, 115422.
- (7) Koshino, M.; McCann, E. Gate-induced interlayer asymmetry in ABA-stacked trilayer graphene. *Phys. Rev. B* **2009**, *79*, 125443.

- (8) Rao, P.; Serbyn, M. Gully quantum Hall ferromagnetism in biased trilayer graphene. *Phys. Rev. B* **2020**, *101*, 245411.
- (9) Zibrov, A. A.; Rao, P.; Kometter, C.; Spanton, E. M.; Li, J. I. A.; Dean, C. R.; Taniguchi, T.; Watanabe, K.; Serbyn, M.; Young, A. F. Emergent Dirac Gullies and Gully-Symmetry-Breaking Quantum Hall States in *ABA* Trilayer Graphene. *Phys. Rev. Lett.* **2018**, *121*, 167601.
- (10) Winterer, F.; Seiler, A. M.; Ghazaryan, A.; Geisenhof, F. R.; Watanabe, K.; Taniguchi, T.; Serbyn, M.; Weitz, R. T. Spontaneous gully-polarized quantum Hall states in *ABA* trilayer graphene. *Nano Letters* **2022**, *22*, 3317–3322.
- (11) Morimoto, T.; Koshino, M. Gate-induced Dirac cones in multilayer graphenes. *Phys. Rev. B* **2013**, *87*, 085424.
- (12) Srivastav, S. K.; Udupa, A.; Watanabe, K.; Taniguchi, T.; Sen, D.; Das, A. Electric-Field-Tunable Edge Transport in Bernal-Stacked Trilayer Graphene. *Phys. Rev. Lett.* **2024**, *132*, 096301.
- (13) Cong, C.; Yu, T.; Sato, K.; Shang, J.; Saito, R.; Dresselhaus, G. F.; Dresselhaus, M. S. Raman Characterization of *ABA*- and *ABC*-Stacked Trilayer Graphene. *ACS Nano* **2011**, *5*, 8760–8768.
- (14) Pizzocchero, F.; Gammelgaard, L.; Jessen, B. S.; Caridad, J. M.; Wang, L.; Hone, J.; Bøggild, P.; Booth, T. J. The hot pick-up technique for batch assembly of van der Waals heterostructures. *Nature Communications* **2016**, *7*, 11894.
- (15) Wang, L.; Meric, I.; Huang, P. Y.; Gao, Q.; Gao, Y.; Tran, H.; Taniguchi, T.; Watanabe, K.; Campos, L. M.; Muller, D. A.; Guo, J.; Kim, P.; Hone, J.; Shepard, K. L.; Dean, C. R. One-Dimensional Electrical Contact to a Two-Dimensional Material. *Science* **2013**, *342*, 614–617.

- (16) Kaur, S.; Chanda, T.; Amin, K. R.; Sahani, D.; Watanabe, K.; Taniguchi, T.; Ghorai, U.; Gefen, Y.; Sreejith, G. J.; Bid, A. Universality of quantum phase transitions in the integer and fractional quantum Hall regimes. *Nature Communications* **2024**, *15*, 8535.
- (17) See Supplemental Material at [URL] for additional figures and details of the sample fabrication and brief description which also includes Refs. ^{26,27}.
- (18) Zou, K.; Zhang, F.; Clapp, C.; MacDonald, A. H.; Zhu, J. Transport Studies of Dual-Gated ABC and ABA Trilayer Graphene: Band Gap Opening and Band Structure Tuning in Very Large Perpendicular Electric Fields. *Nano Letters* **2013**, *13*, 369–373.
- (19) Zhou, H.; Auerbach, N.; Uzan, M.; Zhou, Y.; Banu, N.; Zhi, W.; Huber, M. E.; Watanabe, K.; Taniguchi, T.; Myasoedov, Y.; Yan, B.; Zeldov, E. Imaging quantum oscillations and millitesla pseudomagnetic fields in graphene. *Nature* **2023**, *624*, 275–281.
- (20) Datta, B.; Adak, P. C.; kun Shi, L.; Watanabe, K.; Taniguchi, T.; Song, J. C. W.; Deshmukh, M. M. Nontrivial quantum oscillation geometric phase shift in a trivial band. *Science Advances* **2019**, *5*, eaax6550.
- (21) Koshino, M. Interlayer screening effect in graphene multilayers with *ABA* and *ABC* stacking. *Phys. Rev. B* **2010**, *81*, 125304.
- (22) Slonczewski, J. C.; Weiss, P. R. Band Structure of Graphite. *Phys. Rev.* **1958**, *109*, 272–279.
- (23) McClure, J. Electron energy band structure and electronic properties of rhombohedral graphite. *Carbon* **1969**, *7*, 425–432.
- (24) Assouline, A.; Wang, T.; Zhou, H.; Cohen, L. A.; Yang, F.; Zhang, R.; Taniguchi, T.; Watanabe, K.; Mong, R. S. K.; Zaletel, M. P.; Young, A. F. Energy Gap of the Even-

- Denominator Fractional Quantum Hall State in Bilayer Graphene. *Phys. Rev. Lett.* **2024**, *132*, 046603.
- (25) Volkov, A. V.; Shylau, A. A.; Zozoulenko, I. V. Interaction-induced enhancement of g factor in graphene. *Phys. Rev. B* **2012**, *86*, 155440.
- (26) Venugopal, A.; Chan, J.; Li, X.; Magnuson, C. W.; Kirk, W. P.; Colombo, L.; Ruoff, R. S.; Vogel, E. M. Effective mobility of single-layer graphene transistors as a function of channel dimensions. *Journal of Applied Physics* **2011**, *109*, 104511.
- (27) Amin, K. R.; Nagarajan, R.; Pandit, R.; Bid, A. Multifractal Conductance Fluctuations in High-Mobility Graphene in the Integer Quantum Hall Regime. *Phys. Rev. Lett.* **2022**, *129*, 186802.